

# Dynamic viscoelastic behavior of individual Gram-negative bacterial cells

Virginia Vadillo-Rodriguez<sup>abc</sup> and John R. Dutcher<sup>\*ac</sup>

Received 22nd June 2009, Accepted 11th September 2009

First published as an Advance Article on the web 27th October 2009

DOI: 10.1039/b912227c

We have used atomic force microscopy (AFM) to measure the viscoelastic properties of individual *Escherichia coli* K12 cells under fully hydrated conditions by collecting AFM force-indentation and force-time curves. Spherical colloidal tips were used to reduce the local strain ensuring that the measurements were performed in the linear viscoelastic regime. We find that the cells exhibit a time-dependent viscoelastic response to the constant compressive force applied by the AFM tip. The results are interpreted using the standard solid model which describes both an instantaneous and a delayed elastic deformation. The values obtained for the three viscoelastic parameters were used to generate a full description of the dynamic viscoelastic behavior of the cells over a wide range of frequencies derived from the differential equation governing the standard solid model. The results obtained using this methodology are compared to experimental data obtained for the *E. coli* K12 cells and these results are compared to previously reported viscoelastic data on *Pseudomonas aeruginosa* PAO1 cells. The differences between the viscoelastic behaviors of these two types of Gram-negative bacterial cells are discussed in terms of their structural differences.

## Introduction

A bacterial cell wall separates the crowded interior of the cell from its external environment. The large number of diverse biomolecules that are necessary for cell growth and division create a large pressure difference across the bacterial cell wall. Maintaining this pressure difference is essential for the survival of the cell, and this imposes particularly challenging requirements on the mechanical properties of the cell wall as the cell grows and divides. The mechanical properties of the cell wall also are responsible for the maintenance of cell shape during cell growth. Understanding how the cell shape is regulated in time and space during cell growth and division is a long-standing fundamental problem of contemporary biology and it requires quantitative estimates of cell mechanical properties.

The mechanical properties of the cell wall originate from the structural organization of the constituent molecules, as determined by intermolecular interactions. In Gram-negative cells (e.g. *Escherichia coli* and *Pseudomonas aeruginosa*), the basic structural components of the inner and outer membranes are phospholipids, proteins, and lipopolysaccharide molecules that extend into the extracellular space. The peptidoglycan layer is a covalently linked macromolecular structure composed of stiff glycan chains that are cross-linked by more flexible peptide stems. There are also proteins associated with the peptidoglycan layer, such as lipoproteins, that link it to the outer membrane. Here, the “lipo” substituent is inserted into the hydrophobic domain of the

outer membrane and the “protein” portion is linked to the peptidoglycan by either covalent or electrostatic bonds.<sup>1–3</sup> Loss or altered expression of these proteins has been shown to affect cell shape generation and/or maintenance in *E. coli* strains.<sup>4</sup>

Much of the recent literature on the mechanical properties of intact bacterial cells and their isolated surface layers has focused on qualitative and/or quantitative estimates of their elastic properties.<sup>5–7</sup> Measurements of the deformation of Gram-negative bacterial cells have showed that the peptidoglycan layer inside living cells behaves like a flexible polyelectrolyte gel that swells or shrinks reversibly due to electrostatic forces.<sup>8,9</sup> Mechanical perturbation of the isolated peptidoglycan layer of the *E. coli* and *P. aeruginosa* cells with the tip of an atomic force microscope (AFM) directly demonstrated that this cell surface layer is extensible, flexible and elastic.<sup>10</sup> We have recently shown that intact individual bacterial cells are not purely elastic but have a mechanical response that combines the properties of elastic solids and viscous fluids, and are thus viscoelastic materials.<sup>11,12</sup> In these studies, we applied a constant force to fully hydrated bacterial cells using an AFM tip. Following the rapid indentation of the AFM tip into the bacterial cell, we observed that the tip further indented the cell with time in response to the constant applied force. This time-dependent mechanical response of the cell is the nanoscale equivalent of the creep response observed in bulk engineering materials that is used to determine their viscoelastic properties.<sup>13,14</sup> We interpreted the response of the bacterial cells in terms of the combination of an elastic and a delayed elastic response that can be described by a simple mechanical model called the standard solid model consisting of an elastic spring in series with a parallel combination of a spring and a dashpot.<sup>13</sup> In the AFM creep experiment, the application of the applied force generates force-indentation curves that provide information about the elastic properties of the material when the force is applied relatively quickly, i.e. on a time scale for which viscous contributions are small.<sup>15,16</sup> The

<sup>a</sup>Department of Physics, University of Guelph, Guelph, Ontario, Canada N1G 2W1. E-mail: dutcher@physics.uoguelph.ca; Fax: +1 519 836 9967; Tel: +1 519 824 4120 ext 53950

<sup>b</sup>Department of Molecular and Cellular Biology, University of Guelph, Guelph, Ontario, Canada N1G 2W1

<sup>c</sup>Advanced Foods and Materials Network, Networks of Centres of Excellence (AFMnet), University of Guelph, Guelph, Ontario, Canada N1G 2W1

relationship between the elastic and delayed elastic contributions is obtained by recording force–time curves or creep curves<sup>11</sup> in which the time-dependent displacement (creep) of the AFM tip is measured in response to the constant compressive force that is applied to the cell. From the force–indentation curves and the creep curves, we were able to determine both the instantaneous elastic response and the delayed elastic response characterized by a response time  $\tau$ . This type of experiment has allowed us to characterize the difference in viscoelastic response between Gram-negative and Gram-positive cells, and to quantify the mechanical role of Lpp, the major peptidoglycan-associated lipoprotein and one of the most abundant outer membrane proteins in *E. coli* cells.<sup>12</sup>

In the present study, the viscoelastic properties of individual *E. coli* K12 cells under fully hydrated conditions have been investigated by collecting AFM force–indentation and force–time curves using spherical colloidal tips that reduce the local strain and ensure that the measurements are performed in the linear viscoelastic regime. As for *P. aeruginosa* PAO1 cells,<sup>11</sup> we find that the *E. coli* K12 cells exhibit a viscoelastic solid-like behavior with both an instantaneous and a delayed elastic deformation. The time-dependent response of the *E. coli* K12 cells to a constant applied force is well described by the standard solid model. Best-fit values of the three viscoelastic parameters of the standard solid model, obtained from the force–indentation and creep curves, were used to generate a full description of the dynamic viscoelastic behavior of the cells over a wide range of frequencies derived from the differential equation which governs the standard solid model. The results obtained using this methodology were experimentally corroborated for the *E. coli* K12 cells and compared to previously reported viscoelastic data on *P. aeruginosa* PAO1 cells.<sup>11</sup> The differences between the viscoelastic behavior measured for these two types of Gram-negative cells are discussed in terms of structural differences between the cells.

## Experimental

### Bacterial strain, growth condition, and harvesting

*E. coli* K12 was maintained on Trypticase Soy Agar (TSA, Becton, Dickinson and Company) and cultured in Trypticase Soy Broth (TSB, Becton, Dickinson and Company) for experimentation at 37 °C for 16 h on a rotary shaker (150 rpm) to a late exponential growth phase. Bacteria were harvested by centrifugation (5 min at 1150 × *g*), washed twice and resuspended in deionized water.

### Sample preparation

An important requirement for AFM investigations is that the sample must be immobilized on a surface. For this purpose, an aliquot of bacterial suspension of  $\sim 10^5$  cells per ml was allowed to adhere through electrostatic interactions to a very thin layer of poly-L-lysine on a glass substrate that was prepared as previously described.<sup>7</sup> After 15 min, the bacteria-coated glass substrate was rinsed with Milli-Q water (resistivity of 18.2 M $\Omega$  cm) to remove loosely attached bacteria and then transferred to the AFM for immediate measurement. No cell damage was observed due to osmotic shock following rinsing with Milli-Q water.

### AFM force data acquisition

AFM force measurements were performed using an Asylum MFP-3D AFM (Asylum Research, Santa Barbara, CA) with samples placed under Milli-Q water and held at a temperature of  $34.7 \pm 0.2$  °C, which was the equilibrated temperature within the environmental isolation chamber that enclosed the AFM system. The AFM was controlled using the MFP-3D software provided by the manufacturer that operates within the Igor Pro 6.02A software environment (Wavemetrics, Lake Oswego, OR). OTR4 cantilevers with colloidal silicon oxide tips with a tip radius of 300 nm (Novascan Technologies, Inc.) were used to collect force–distance and force–time curves. Prior to use, the spring constant of each cantilever was determined using the thermal fluctuation method.<sup>17</sup> Typically, the cantilever spring constant was  $0.07 \pm 0.01$  N m<sup>-1</sup>. To locate the center of the top of the bacterial cells, AFM topographic images of the cells, which had lengths of  $2.1 \pm 0.4$   $\mu$ m and widths of  $0.8 \pm 0.1$   $\mu$ m, were recorded in contact mode at low applied force ( $\sim 1$  nN) using a scan rate of 1 Hz. For force–distance curve acquisition, the AFM tip was lowered at a specific rate toward the center of the top of individual cells until a preset value of the loading force  $F_0$  was reached, followed by immediate retraction of the tip at the same rate. In force–time or creep curves, however, the loading force  $F_0$  was held constant for a 10 s period prior to retraction of the tip by controlling the cantilever deflection  $d$ , where  $F_0 = kd$  and  $k$  is the cantilever spring constant, and the cantilever base displacement ( $Z$ ) was measured during the contact period by monitoring the vertical movement of the  $z$ -piezoelectric transducer. For samples, such as bacterial cells, that are less stiff than the cantilever, the deflection of the cantilever during the approach of the AFM tip to the sample can be assumed to result exclusively from the mechanical indentation of the cell.<sup>11</sup> Because of this, force–distance curves were used to generate force–indentation curves according to the method described in ref. 15,16. The  $Z$  data collected during the time of contact between the AFM tip and the bacterial cell in force–time curves represents the time-dependent deformation of the bacterial cell in the presence of a constant loading force, *i.e.* the cell creep response. For creep curves, the first data point was taken as the indentation ( $z_0$ ) measured from the corresponding approach force–indentation curve just after the desired load  $F_0$  was reached. A more detailed description of force–distance and force–time curve acquisition and interpretation can be found in ref. 11,18.

To investigate the dependence of the cell creep response on the magnitude of the loading force,  $F_0$  was varied between 2 and 10 nN in the experiments. Three force–time curves were collected per cell for each value of the applied force, and six cells from two different cultures were studied. Thus, the cell viscoelastic parameters reported in this study were calculated as the average of the values obtained from the analysis of eighteen force–time curves for each experimental condition. For the same number of cells, a set of force–distance curves were recorded at a constant applied force of 6 nN while varying the loading rate between 0.35 and 72 nN s<sup>-1</sup>. These curves were used to investigate the dependence of the cell mechanical response on the loading rate or frequency. Note that for each loading rate the corresponding frequency  $\omega$  in rad s<sup>-1</sup> was calculated as  $\pi$  divided by the time needed to achieve the preset load of 6 nN.

Consecutive force–distance and force–time curves were very reproducible, indicating that there was no plastic deformation (*i.e.* irreversible deformation) taking place on the time scale of the measurements. As a control, force–distance and force–time curves were also recorded on clean glass substrates for each experimental condition investigated.

Force–distance and force–time curves were exported into data files using the MFP-3D software and analyzed using the Advance Fitting Tool provided within the Origin 7.0 software package (OriginLab, Northampton, MA).

### Analysis of the cell viscoelastic parameters and their dependence on frequency

The viscoelastic behavior of materials can be modeled as combinations of elastic elements (springs) and viscous elements (dashpots).<sup>13</sup> These models are used to derive equations that describe the deformation of the material under investigation. One of the simplest models that predict creep behavior is called the standard solid,<sup>19</sup> which is shown schematically in Fig. 1. It consists of an elastic spring, which describes an instantaneous elastic deformation, placed in series with a parallel combination of a spring and dashpot (Kelvin–Voigt element), which describes a delayed elastic deformation. We have used the standard solid model to interpret the creep data obtained on bacterial cells in the present study since we obtain evidence for both an elastic and a delayed elastic response. We have not allowed for the possibility of viscous flow because the deformations observed in the present experiments are reversible, to within the precision of the experiment. Based on the standard solid model, we have derived the following equation that we have used to describe the experimentally observed creep response:

$$Z(t) = \frac{F_0}{k_1} + \frac{F_0}{k_2} \left[ 1 - \exp\left(-t \frac{k_2}{\eta_2}\right) \right] \quad (1)$$

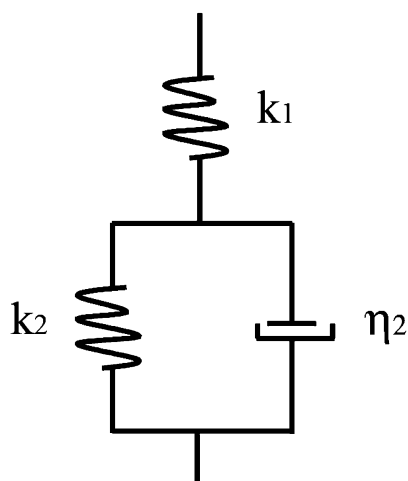


**Fig. 1** Schematic diagram of the standard solid model used to obtain the cell viscoelastic constants. The model consists of an elastic spring with stiffness  $k_1$ , which describes the instantaneous elastic deformation, in series with a parallel combination of a spring with stiffness  $k_2$  and a dashpot with viscosity  $\eta_2$ , which describes the delayed elastic deformation.

where  $Z(t)$  is the position of the  $z$ -piezoelectric transducer as a function of time  $t$ ,  $F_0$  is the magnitude of the loading force, and  $k_1$  and  $k_2$  are the spring constants and  $\eta_2$  is the viscosity characterizing the cell surface. The ratio  $\eta_2/k_2$  is the so-called characteristic response time  $\tau$  corresponding to the time during which the sample deforms by  $1 - e^{-1}$  (or 63.2%) of the total creep-deformation. The fits of the creep-deformation data to this model were found to be very good, with linear correlation coefficient values that are close to one ( $R^2 \geq 0.96$ ).

To obtain a full understanding of the viscoelastic properties of a material, the material has to be characterized over a wide range of frequencies. Analysis of the differential equation describing the standard solid model can be used to determine analytical expressions for the elastic and viscous response of a material as a function of frequency. The governing differential equation of the standard solid model can be expressed as:<sup>19,20</sup>

$$\frac{dF(t)}{dt} + \frac{k_1 + k_2}{\eta_2} F(t) = k_1 \frac{dZ(t)}{dt} + \frac{k_1 k_2}{\eta_2} Z(t) \quad (2)$$

where  $k_1$ ,  $k_2$  and  $\eta_2$  are the material constants of the standard solid model (see Fig. 1) and  $F(t)$  and  $Z(t)$  are the time-dependent force and deformation, respectively. To solve this differential equation, we assume that  $F(t) = F_0 e^{i\omega t}$  and the resulting deformation  $Z(t) = Z_0 e^{i(\omega t - \delta)}$ , where  $\delta$  is the phase shift between the driving force and the deformation. Substituting these expressions into eqn (2) yields:

$$F(t) \left[ i\omega + \frac{k_1 + k_2}{\eta_2} \right] = Z(t) \left[ i\omega k_1 + \frac{k_1 k_2}{\eta_2} \right] \quad (3)$$

Rearranging eqn (3) we obtain an expression for the time-dependent mechanical response of the viscoelastic material  $E^*(\omega)$ :

$$\frac{F(t)}{Z(t)} = \frac{i\omega \eta_2 k_1 + k_1 k_2}{i\omega \eta_2 + k_1 + k_2} = E^*(\omega) = E_1(\omega) + iE_2(\omega) \quad (4)$$

The real part of the mechanical response  $E_1(\omega)$  describes the elastic behavior of the material, and the imaginary part  $E_2(\omega)$  describes the viscous behavior of the material. Eqn (4) can be separated into its real and imaginary parts to yield:

$$E_1(\omega) = \frac{\omega^2 \eta_2^2 k_1 + k_1 k_2 (k_1 + k_2)}{(k_1 + k_2)^2 + \omega^2 \eta_2^2} \quad (5)$$

$$E_2(\omega) = \frac{\omega \eta_2 k_1^2}{(k_1 + k_2)^2 + \omega^2 \eta_2^2} \quad (6)$$

We note that  $E_1$  and  $E_2$  are expressed in  $\text{N m}^{-1}$  and are proportional to the so-called storage and loss moduli, which are typically expressed in Pa or  $\text{N m}^{-2}$ .<sup>21,22</sup>  $E_1(\omega)$  is a sigmoidal function of  $\omega$  and  $E_2(\omega)$  is a peaked function of  $\omega$  for which the maximum slope of  $E_1(\omega)$  and the maximum value of  $E_2(\omega)$  occurs for  $\omega = (k_1 + k_2)/\eta_2$ . The dissipated energy  $W_2$  in units of joules can be obtained by multiplying  $E_2$  by  $\pi x_0^2$ .<sup>13,19</sup> Note that for comparison with experimental data, we have plotted  $E_1$  and  $W_2$  as a function of frequency rather than plotting the storage and loss compliance as a function of frequency. It is the compliances that are typically plotted in creep experiments and they represent the mathematical inverse of the storage and loss moduli discussed above.<sup>19</sup>

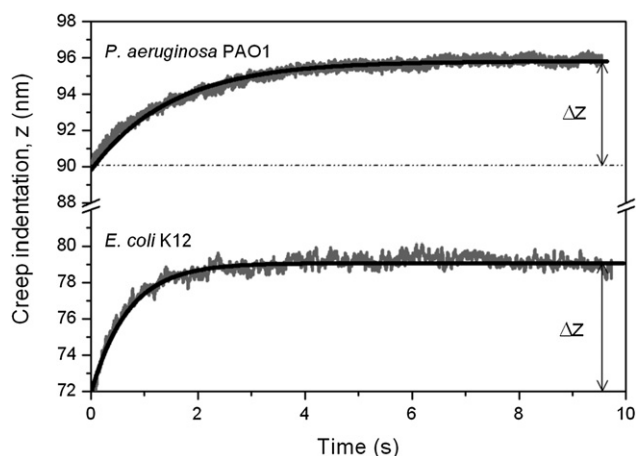


**Fig. 2** Creep indentation measured as a function of time for an *E. coli* K12 cell subjected to a constant applied force of 4 nN. For the sake of comparison, previously reported creep-deformation data of a *P. aeruginosa* PAO1 cell for the same value of applied force have been included. The solid lines were calculated using the best-fit parameter values listed in Table 1 for each data set. The total creep (or delayed elastic) deformation experienced by the cells is indicated in the figure as  $\Delta z$ .

## Results

### Analysis of creep-deformation curves: cell viscoelastic parameters

The force *versus* time data collected during the contact period between the AFM tip and the bacterial cell show that the cells undergo a time-dependent deformation in response to the constant applied force, *i.e.* they creep. Fig. 2 shows an example of creep curves for an applied force of 4 nN. It can be seen that creep-deformation of *E. coli* K12 cells increased monotonically with time, asymptotically approaching an equilibrium value  $\Delta z$  that was achieved within the 10 s time period for data acquisition. For comparison, previously reported creep data<sup>11</sup> of another Gram-negative cell, *P. aeruginosa* PAO1, have been included in Fig. 2. For the creep curves, the first data point corresponds to the time at which the preset loading force  $F_0$  and the initial deformation  $z_0$  were attained. Thus the total cell deformation is the sum of two distinct contributions:  $z_0$ , which is the immediate elastic deformation; and  $\Delta z$ , the overall delayed elastic deformation generated during the 10 s period for the application of the constant force was directly proportional to the loading force (data not shown), indicating that the experiments were performed within the linear viscoelastic regime.

Since we obtained evidence for both an elastic and a delayed elastic response when investigating the mechanical behavior of *E. coli* K12 cells, we have used the standard solid model to extract the cell viscoelastic parameters, *i.e.*  $k_1$ ,  $k_2$  and  $\eta_2$  as defined in eqn (1) and Fig. 1. An example of the best-fit of the standard solid model to typical creep-deformation data is shown in Fig. 2. The average values of the best-fit parameters obtained for different values of the loading force  $F_0$  have been listed in Table 1, since the values do not vary significantly with the value of  $F_0$ . This result verifies that our experiments were carried out within the linear viscoelastic regime. The spring constant  $k_1$  is a measure of

**Table 1** Summary of the best-fit viscoelastic constants of bacterial cells obtained from a least squares fit of the experimental creep response of the cells to eqn (1) derived from the standard solid model (see Fig. 1). The parameters  $k_1$  and  $k_2$  are the stiffness values of the elastic springs,  $\eta_2$  is the viscosity of the dashpot, and  $\tau$  is the characteristic response time defined as the ratio  $\eta_2/k_2$ . The average values of the best-fit parameters obtained for the different values of the loading force  $F_0$  (2, 4, 6 and 10 nN) have been listed, since the values do not vary significantly with the value of  $F_0$

	<i>E. coli</i> K12	<i>P. aeruginosa</i> PAO1 <sup>a</sup>
$k_1/\text{N m}^{-1}$	$0.056 \pm 0.008$	$0.044 \pm 0.002$
$k_2/\text{N m}^{-1}$	$0.54 \pm 0.13$	$0.81 \pm 0.08$
$\eta_2/\text{N}\cdot\text{s m}^{-1}$	$0.36 \pm 0.05$	$1.37 \pm 0.27$
$\tau/\text{s}$	$0.64 \pm 0.08$	$1.82 \pm 0.20$

<sup>a</sup> Data obtained from ref. 11.

the effective spring constant of the sample and it determines the instantaneous elastic deformation ( $z_0$ ) obtained with the rapid application of an applied force  $F_0$  (see more details below). The ratio of the spring constant  $k_2$  to the dashpot viscosity  $\eta_2$  determines the time  $\tau = \eta_2/k_2$  which characterizes the delayed elastic response. For *E. coli* K12 and *P. aeruginosa* PAO1 cells,  $\tau$  is 0.64 and 1.82 s, respectively, indicating that the *E. coli* K12 cells reach their equilibrium creep-deformation faster than the *P. aeruginosa* PAO1 cells (see Fig. 2). The spring constant  $k_2$  also dictates the extent of the overall delayed elastic deformation  $\Delta z$  with a larger value of  $k_2$  producing a smaller value of  $\Delta z$ . Note that in the creep experiments the applied force was ramped at a constant rate of  $72 \text{ nN s}^{-1}$  which is equivalent to a frequency of  $\omega = 38 \text{ rad s}^{-1}$ . For the loading forces investigated (2, 4, 6 and 10 nN), this is equivalent to a total loading time that varies from 0.027 to 0.138 s. This time is substantially smaller than the characteristic time constant  $\tau$  of the cell, and for this reason, the mechanical response of the cell can be separated into two components: an instantaneous elastic response followed by a delayed elastic response due to creep-deformation.

### Dependence of cell mechanical response on loading rate

The cell viscoelastic parameters presented in Table 1 were substituted into eqn (5) and (6) to generate plots of the elastic ( $E_1$ ) and viscous ( $W_2$ ) response of the *E. coli* K12 cells *versus* frequency. In Fig. 3a and b, the solid lines show that at low and high frequencies the elastic storage constant  $E_1$  is independent of frequency and the energy loss  $W_2$  approaches zero. These two regimes, corresponding to low and high loading rates, correspond to the rubbery and glassy states of the material, respectively. In the intermediate regime, corresponding to times that coincide with the characteristic time constant  $\tau$  of the cell,  $E_1$  increases monotonically with increasing frequency and the energy loss  $W_2$  achieves a local maximum.

Although this approach yields a full description of the dynamic viscoelastic behavior of the cells over a wide range of frequencies, we need to validate the methodology by comparing calculated curves of  $E_1(\omega)$  and  $W_2(\omega)$  to experimental data. For this purpose, a set of force–distance curves were collected at several different loading rates that varied between  $0.72$  and  $72 \text{ nN s}^{-1}$ , which is equivalent to a range of effective frequencies of  $0.38$  to  $38 \text{ rad s}^{-1}$ . The approach portion of these curves was used to generate plots of loading force *versus* indentation. An example

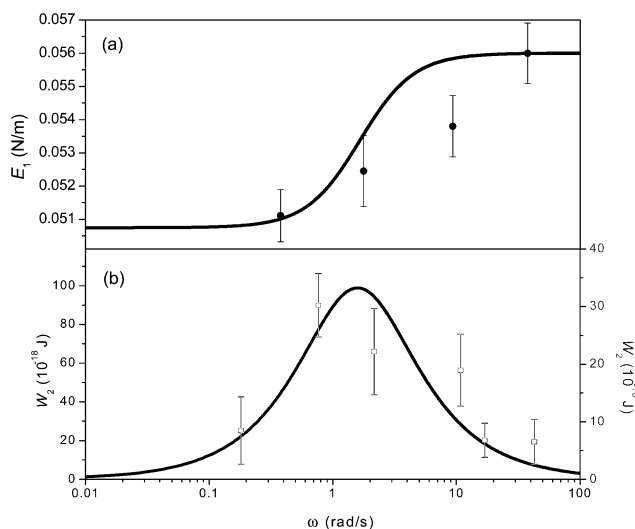


**Fig. 3** Plot of (a) the storage elastic constant  $E_1$  (elastic response) and (b) the energy loss  $W_2$  (viscous response) versus the effective frequency  $\omega$  plotted on a logarithmic scale for *E. coli* K12 cells. The solid lines were calculated using eqn (5) and (6), respectively, and the best-fit viscoelastic parameters listed in Table 1. The  $E_1$  data points are average values ( $n = 5$ – $10$ ) of the effective cell spring constant  $k_{\text{eff}}$  as derived from the approach portion of force-indentation curves, and the error bars correspond to the standard deviation of the  $k_{\text{eff}}$  values obtained at each value of the effective frequency. The  $W_2$  data points are average values ( $n = 3$ – $6$ ) of the area enclosed between the loading and unloading lines in the force-indentation curves obtained at different effective frequencies.

of force-indentation curves for an applied force of 6 nN and effective frequencies of 0.38, 1.8, 9.4, and 38 rad s<sup>-1</sup> is shown in Fig. 4. For all frequencies, the cell response to the loading force is essentially linear, corresponding to an elastic response, and therefore an effective cell spring constant ( $k_{\text{eff}}$ ) can be readily estimated by calculating the ratio between the loading force and the depth of indentation. As expected for a viscoelastic system, the rigidity of the cell increases with increasing frequency for frequencies  $\omega$  that are comparable to  $(k_1 + k_2)/\eta_2$  (see the  $E_1$  data points in Fig. 3) and we see that the increase of  $k_{\text{eff}}$  over the

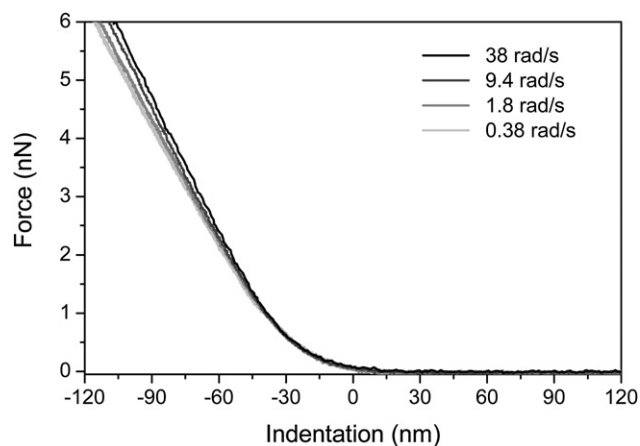


**Fig. 4** Approach force-indentation curves obtained for *E. coli* K12 cells for an applied force of 6 nN and for loading rate values that ranged between 0.38 and 38 rad s<sup>-1</sup>.

effective frequency range of the measurements agrees quite well with the storage elastic constant  $E_1$  as defined in eqn (5). It is important to note that at an effective frequency of 38 rad s<sup>-1</sup>, the time for the application of the applied force is very small compared to the cell characteristic time (0.084 vs. 0.64 s) and thus, at this loading rate, the cell undergoes a rapid, elastic deformation (indentation =  $z_0$ ) and  $k_{\text{eff}}$  corresponds to  $k_1$  ( $k_{\text{eff}} = k_1 = 0.056 \text{ N m}^{-1}$ ).

As the loading time increases and the effective frequency decreases, the time required to achieve the desired load becomes comparable to or larger than the characteristic time  $\tau$  of the cell. Therefore, substantial relaxation of the cell wall occurs during the application of the applied force in addition to the instantaneous elastic deformation. As a result of this additional relaxation during the approach of the AFM tip, larger values of the indentation are measured during the approach (see Fig. 4) corresponding to smaller values of the effective cell spring constant  $k_{\text{eff}}$ . When the time required to withdraw the tip from the cell is comparable to or larger than the characteristic time  $\tau$  of the cell, the cell undergoes creep-deformation during the unloading process. This results in a difference in the force-displacement behavior observed during loading and unloading, with the area of the loop on the force-displacement plot equal to the fraction of the delayed elastic energy (or 'energy loss') that accumulates during the unloading process. We can directly measure this area on the force-indentation curves obtained for the approach and retraction of the AFM tip. An example of these curves is shown in Fig. 5a and b for loading/unloading effective frequencies of

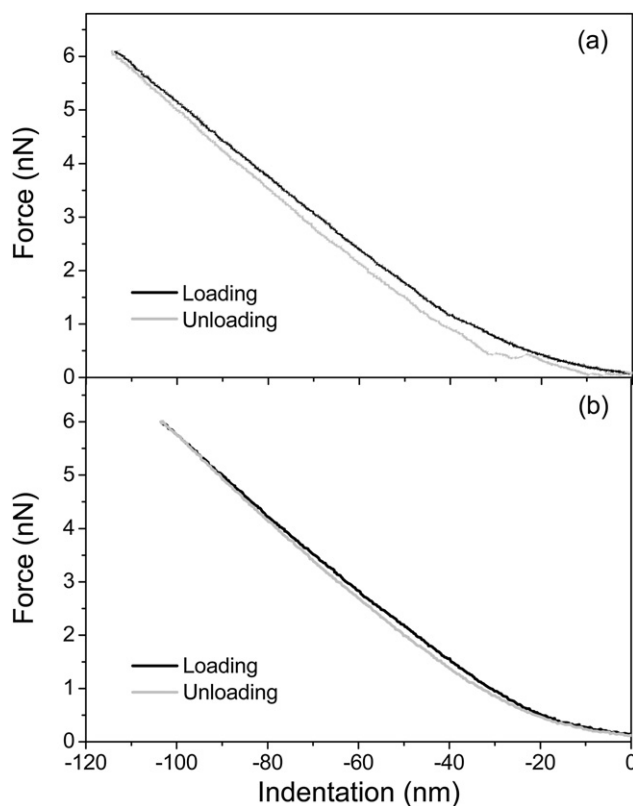


**Fig. 5** Force-indentation curves (both loading and unloading lines are displayed) obtained for *E. coli* K12 cells using loading-unloading effective frequencies  $\omega$  of (a) 0.38 rad s<sup>-1</sup> and (b) 38 rad s<sup>-1</sup>.

0.38 rad s<sup>-1</sup> and 38 rad s<sup>-1</sup>, respectively. When compared to the ‘energy loss’  $W_2$  as defined in eqn (6) we found that the experimental data (see the  $W_2$  data points in Fig. 3) qualitatively reproduced the frequency dependence of  $W_2$  within the range of effective frequencies investigated. Quantitatively, however, the experimental data underestimate the calculated values of the maximum ‘energy loss’ by a factor of 2.5. This discrepancy is perhaps not surprising since the force–indentation curves of *E. coli* K12 cells (see Fig. 5a and b) show a very small delayed deformation, which is responsible for the hysteresis loop, on a background of a large elastic deformation. For this reason, it is very difficult to isolate the magnitude of the delayed deformation with a high degree of accuracy using this method of measurement. Nevertheless, the experimental data showed that at low and high frequencies the energy loss approaches zero as expected, indicating that the unloading line follows the loading line at the two extremes of the frequency range. This is because at very low frequencies the cell has enough time to experience the total creep-deformation during the loading–unloading cycle, whereas at very high frequencies the cell does not have enough time to experience any creep-deformation during this cycle.

#### Dynamic viscoelastic behavior of *E. coli* K12 versus *P. aeruginosa* PAO1

To compare the dynamic viscoelastic behavior obtained for *E. coli* K12 cells, previously reported viscoelastic constants for *P. aeruginosa* PAO1<sup>11</sup> were used to calculate plots of the storage elastic constant  $E_1$  and the ‘energy loss’  $W_2$  as a function of frequency (see Fig. 6). For the same value of the loading rate, *P. aeruginosa* PAO1 cells are less stiff and have a smaller value of the ‘energy loss’ than the *E. coli* cells (comparing the black and grey curves in Fig. 6). This latter result indicates that *P. aeruginosa* PAO1 cells offer more resistance to deformation, and hence, they are more viscous, than *E. coli* K12 cells. As well, it can be seen that the maximum of  $W_2$  is shifted to smaller frequencies for

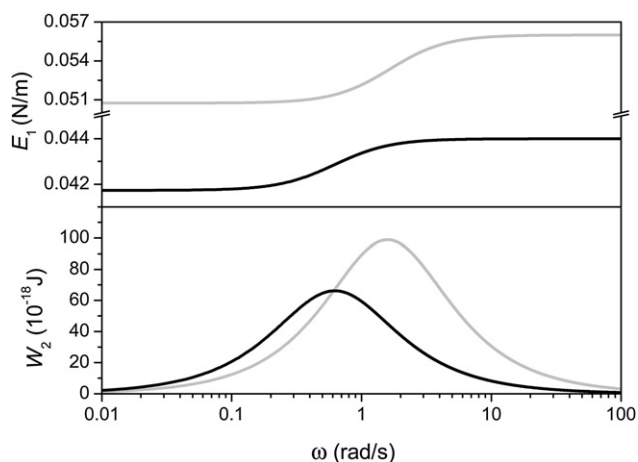


**Fig. 6** Storage elastic constant  $E_1$  and energy loss  $W_2$  as a function of the effective frequency  $\omega$  plotted on a logarithmic scale for *P. aeruginosa* PAO1 cells (black curves), calculated using eqn (5) and (6) together with the cell viscoelastic constants listed in Table 1. We have also plotted the curves calculated for *E. coli* K12 cells (grey curves) from Fig. 3 for comparison.

*P. aeruginosa* PAO1, corresponding to the larger characteristic response time measured for the *P. aeruginosa* PAO1 cells.

## Discussion

It is important to understand the mechanical behavior of bacterial cells in view of the significant role that mechanical properties play in the physiological processes of the cells. For example, the dynamics of cell growth and division involve large deformations of the cell envelope. In addition, the passage of small molecules across the membrane is likely to induce transient nanoscale deformations of the cell envelope. Both of these processes must occur in response to locally generated forces without compromising the mechanical integrity of the cell envelope so that turgor pressure can be maintained. In the present study, we have imposed a local compressive stress on the bacterial cells by pressing an AFM tip into *E. coli* K12 bacterial cells and measured the mechanical response of the cells to the force. We find that the response of the cells is viscoelastic, made up of both elastic and delayed elastic contributions, and that these contributions depend on the rate at which the force is applied. The relative importance of the elastic and delayed elastic contributions to the mechanical response of the cells will depend on the specific composition and interactions between the molecules within the cell envelope. To separate the contributions of, e.g., the cell membrane and the peptidoglycan, it is necessary to measure the mechanical properties of the isolated surface layer components as well as the bacterial cells under fully hydrated conditions.

Typically, the rigidity of the bacterial cell envelope has been attributed solely to the peptidoglycan layer. This concept arose because the disruption of the cell envelope of rod-shaped bacteria with chemical treatments resulted in the formation of round, osmotically sensitive cells called spheroplasts, whereas the isolated peptidoglycan sacculi retained the rod shape of intact cells.<sup>23–25</sup> Later studies showed that by varying the net charge on the *E. coli* sacculi *in vivo* and *in vitro*, they could be expanded and contracted reversibly over a four-fold range in area, revealing the elastic nature of the peptidoglycan layer.<sup>26</sup> Yao *et al.*<sup>10</sup> assessed the elastic properties of isolated, hydrated *E. coli* K12 and *P. aeruginosa* PAO1 sacculi using AFM nanoindentation experiments. They reported that the hydrated sacculi rebounded without hysteresis after the AFM tip pressure was removed, suggesting that the sacculi are elastic materials. Although *P. aeruginosa* sacculi appeared to be more deformable than *E. coli* sacculi during AFM scanning in their experiments, a similar elastic modulus of  $\sim 2.5 \times 10^7$  Pa was obtained for both *E. coli* and *P. aeruginosa* sacculi. In contrast, we have found *P. aeruginosa* PAO1 cells are less stiff than *E. coli* K12 cells (see the values of the elastic constant  $E_1$  in Fig. 3 and 6) over the entire range of loading rates or effective frequencies investigated. It is reasonable to assume that the elastic strength of the cells depends on the thickness of their peptidoglycan layer (assuming that the degree of cross-linking between adjacent glycan chains is similar between the strains), and frozen-hydrated thin sections of *E. coli* K12 and *P. aeruginosa* PAO1 cells imaged using cryo-transmission electron microscopy have shown that the thickness of the sacculi of *P. aeruginosa* PAO1 cells is three times smaller than that of the *E. coli* K12 cells (2.41 nm versus 6.35 nm,

respectively).<sup>27</sup> The nature of the bonding between the outer membrane and the peptidoglycan layer may also play a role in defining the rigidity of the cell envelope. In *E. coli* K12 cells the outer membrane is covalently linked to the peptidoglycan layer, whereas in *P. aeruginosa* PAO1 cells the layers are linked by a weaker, electrostatic bond.<sup>2,3</sup> Since the experiments to date have indicated that the peptidoglycan layer of Gram-negative cells is predominantly an elastic material, it is tempting to suggest that the elastic contribution to the viscoelastic response of the bacterial cells is dominated by the properties of the peptidoglycan. We note that in the present study we found that a large elastic deformation dominated a small viscous component in the viscoelastic response of the cells (see Fig. 5a and b for example).

Even though the peptidoglycan layer may dictate the elasticity of the cells, our AFM measurements show that lipid membranes can also withstand large, reversible deformations without apparent disruption of the cell. This is perhaps surprising since lipid bilayers can deform only slightly (between 2 and 5%) before rupturing or buckling under compression.<sup>28,29</sup> It has been proposed that in living cells membrane curvature is generated by specialized proteins that are bound to or inserted into the lipid bilayer, and that the energy associated with their adsorption is stored as elastic energy in the membrane.<sup>30,31</sup> Garten and Henning<sup>32</sup> reported a substantial protein–protein interaction in the outer membrane of *E. coli* cells and this is likely true for *P. aeruginosa* cells as well since the envelope of both strains has been shown to consist of 45–50% proteins.<sup>33,34</sup> Although this protein–protein interaction should give rise to the elastic response of the membranes, we believe that the main contribution of the membranes to the viscoelastic response of the bacterial cells is due to their fluidity.

At the nanoscale, components of the membrane such as phospholipids and lipopolysaccharide (LPS) molecules are constantly in motion. They move at high speeds laterally around the cell while rotating along their long axis. It is this movement that gives membrane bilayers their liquid-like character. Because of the inertia of this motion and the viscous properties of the bilayer itself, it is likely that a bilayer will manifest resistance to deformation upon the application of an external force. We find that the values of  $W_2$ , representing the viscous response of the cells, are larger for the *E. coli* K12 cells than the *P. aeruginosa* PAO1 cells over the entire range of loading rates investigated (compare the black and grey curves in Fig. 6). This means that the *E. coli* K12 cells offer less resistance to deformation than *P. aeruginosa* PAO1 cells. A number of properties will affect the viscous response and fluidity of the cell membranes, including bilayer thickness, hydration state of the lipid head groups, interfacial polarity and charge, and coupling between the two monolayers within the membrane bilayer.

The lipopolysaccharide (LPS) molecules within the outer membranes of Gram-negative bacterial cells can also affect the viscous response and fluidity of the membranes. An LPS molecule consists of a lipid A molecule, a short core oligosaccharide, and an O antigen that may be a long polysaccharide. In *P. aeruginosa* cells the lipid A moiety that anchors the LPS to the outer membrane of the cells has been shown to contain shorter fatty acids than the lipid A in *E. coli*.<sup>35</sup> As if to compensate for the decreased intermolecular hydrophobic interactions due to the shorter fatty acid chains, the total number of free OH groups is

increased from two or three in the *E. coli* cells to five or six in *P. aeruginosa* cells, greatly increasing the possibility of stabilization of the LPS leaflet through H-bonding.<sup>36</sup> Divalent cations (e.g.,  $\text{Ca}^{2+}$  and  $\text{Mg}^{2+}$ ) are also thought to provide intra- and intermolecular salt linkages to help stabilize the LPS molecules.<sup>37</sup> The *P. aeruginosa* core oligosaccharide underlying each O-side chain carries more formal negative charges than does the *E. coli* core,<sup>36</sup> and thus it provides more anionic sites for the stabilization of LPS through divalent cations. Clearly, a strong lateral interaction between LPS molecules will decrease the fluidity of the membrane, resulting in a larger resistance to deformation. This could partly explain the higher viscosity values that we observed for *P. aeruginosa* PAO1 cells compared to *E. coli* K12 cells (see values of  $\eta_2$  in Table 1). Another factor that has been shown to have a direct impact on membrane viscosity is the length of the LPS molecules. Yeh and Jacobs<sup>38</sup> found that, when added to phosphatidylcholine liposomes, the LPS fraction containing long O-side chains decreased the fluidity of the phospholipid bilayer more effectively than did the fraction with short or no side chains. Furthermore, it was demonstrated with intact bacterial cells that the lateral diffusion of a particular outer membrane protein (IcsA) becomes faster in a mutant that cannot synthesize the LPS O-side chain.<sup>39</sup> The *E. coli* bacterium used in the present study is a K12 strain for which the LPS is semirough: it consists of lipid A and core oligosaccharide with no O-side chains. In contrast, the LPS of the *P. aeruginosa* PAO1 cells used in the present study is smooth and contains O-side chains.<sup>40</sup> Accordingly, the fluidity of the *P. aeruginosa* PAO1 membrane is expected to be lower than that of *E. coli* K12 and this is again in agreement with our observations.

In summary, we have demonstrated through AFM force–indentation and force–time curves that the response of Gram-negative *E. coli* cells to an imposed external force is made up of both elastic and delayed elastic contributions, and that these depend on the rate at which the force is applied. For the first time, a full description of the dynamic viscoelastic behavior of cells over a wide range of frequencies was obtained based on an analysis of the differential equation governing the standard solid model and the calculated frequency dependence of the viscoelastic properties was corroborated with experimental data. Comparison of the results obtained for *E. coli* K12 cells with previously reported data on the mechanical properties of Gram-negative bacterial cells and their isolated peptidoglycan layers suggests that the elastic component of the viscoelastic response of the cells is likely dominated by the properties of the peptidoglycan layer, whereas the viscous component likely arises from the liquid-like character of the cell membranes. This work represents a new attempt to understand how molecular structure is related to the cell mechanical properties, which could be of practical value in elucidating the biomechanical effects of drugs on pathogens. In addition, these measurements have the potential to help elucidate mechanical signal transduction pathways once the cell mechanical properties are correlated with physiological processes.

## Acknowledgements

The authors gratefully acknowledge financial support from the Advanced Foods and Materials Network (AFMnet), the Canada

Foundation for Innovation and the Natural Sciences and Engineering Research Council of Canada. JRD acknowledges support from the Canada Research Chairs (CRC) program. This work is dedicated to the late Terry Beveridge, our good friend and superb colleague, who provided the motivation for this work.

## References

- 1 M. T. Cabeen and C. Jacobs-Wagner, *Nat. Rev. Microbiol.*, 2005, **3**, 601–610.
- 2 T. J. Beveridge, *Int. Rev. Cytol.*, 1981, **72**, 229–317.
- 3 R. E. W. Hancock, R. Siehnel and N. Martin, *Mol. Microbiol.*, 1990, **4**, 1069–1075.
- 4 I. Sonntag, H. Schwarz, Y. Hirota and U. Henning, *J. Bacteriol.*, 1978, **136**, 280–285.
- 5 X. Yao, J. Walker, S. Burke, S. Stewart, M. H. Jericho, D. Pink, R. Hunter and T. Beveridge, *Colloids Surf., B: Biointerfaces*, 2002, **23**, 213–230.
- 6 W. Xu, P. J. Mulhern, B. L. Blackford, M. H. Jericho, M. Firter and T. J. Beveridge, *J. Bacteriol.*, 1996, **178**, 3106–3112.
- 7 L. Zhao, D. Schaefer and M. R. Marten, *Appl. Environ. Microbiol.*, 2005, **71**, 955–960.
- 8 R. E. Marquis, *J. Bacteriol.*, 1968, **95**, 775–781.
- 9 L.-T. Ou and R. E. Marquis, *J. Bacteriol.*, 1970, **101**, 92–101.
- 10 X. Yao, M. Jericho, D. Pink and T. Beveridge, *J. Bacteriol.*, 1999, **181**, 6865–6875.
- 11 V. Vadillo-Rodriguez, T. J. Beveridge and J. R. Dutcher, *J. Bacteriol.*, 2008, **190**, 4225–4232.
- 12 V. Vadillo-Rodriguez, S. R. Schooling and J. R. Dutcher, *J. Bacteriol.*, 2009, **191**, 5518–5525.
- 13 I. M. Ward and D. W. Hadley, *An Introduction to the Mechanical Properties of Solid Polymers*, John Wiley & Sons, Hoboken, NJ, 1993.
- 14 J. D. Ferry, *Viscoelastic Properties of Polymers*, John Wiley & Sons, Hoboken, NJ, 3rd edn, 1980.
- 15 M. Arnoldi, C. M. Kacher, E. Bauerlein, M. Radmacher and M. Fritz, *Appl. Phys. A*, 1998, **66**, S613–S617; M. Arnoldi, M. Fritz, E. Bauerlein, M. Radmacher, E. Sackmann and A. Boulbitch, *Phys. Rev. E: Stat. Phys., Plasmas, Fluids, Relat. Interdiscip. Top.*, 2000, **62**, 1034–1044.
- 16 M. Radmacher, M. Fritz and P. K. Hansma, *Biophys. J.*, 1995, **69**, 264–270.
- 17 R. Levy and M. Maaloum, *Nanotechnology*, 2002, **13**, 33–37.
- 18 A. A-Hassan, W. F. Heinz, M. D. Antonik, N. P. D'Costa, S. Nageswaran, C. A. Schoenberger and J. H. Hoh, *Biophys. J.*, 1998, **74**, 1564–1578.
- 19 W. N. Findley, J. S. Lai and K. Onaran, *Creep and Relaxation of Nonlinear Viscoelastic Materials with an Introduction to Linear Viscoelasticity*, Dover Publications, Inc., New York, NY, 1989.
- 20 M. Qaisar, *Pure Appl. Geophys.*, 1989, **131**, 703–713.
- 21 T. Wakatsuki, M. S. Kolodney, G. I. Zahalk and E. L. Elson, *Biophys. J.*, 2000, **79**, 2353–2368.
- 22 F. Gittes, B. Schnurr, P. D. Olmsted, F. C. MacKintosh and C. F. Schmidt, *Phys. Rev. Lett.*, 1997, **79**, 3286–3289.
- 23 J. Lederberg, *Biochemistry*, 1956, **42**, 574–577.
- 24 W. Weidel and H. Pelzer, *Adv. Enzymol. Relat. Areas Mol. Biol.*, 1964, **26**, 193–232.
- 25 W. Weidel, W. H. Frank and H. H. Martin, *J. Gen. Microbiol.*, 1960, **22**, 158–166.
- 26 A. L. Koch and S. Woeste, *J. Bacteriol.*, 1992, **174**, 4811–4819.
- 27 V. R. F. Matias, A. Al-Amoudi, J. Dubochet and T. J. Beveridge, *J. Bacteriol.*, 2003, **185**, 6112–6118.
- 28 A. L. Koch, *Crit. Rev. Microbiol.*, 1998, **24**, 23–59.
- 29 H. J. Butt and V. Franz, *Phys. Rev. E: Stat. Phys., Plasmas, Fluids, Relat. Interdiscip. Top.*, 2002, **66**, 0316011–0316019.
- 30 M. M. Kozlov, *Nature*, 2007, **447**, 387–389.
- 31 B. J. Reynwar, G. Illya, V. A. Harmandaris, M. M. Muller, K. Kremer and M. Deserno, *Nature*, 2007, **447**, 461–464.
- 32 W. Garten and U. Henning, *Eur. J. Biochem.*, 1974, **47**, 343–352.
- 33 K. Clarke, G. W. Gray and D. A. Reaveley, *Biochem. J.*, 1967, **105**, 749–754.
- 34 R. E. W. Hancock and H. Nikaïdo, *J. Bacteriol.*, 1978, **136**, 381–390.
- 35 V. A. Kulshin, U. Zahringer, B. Lindner, K. E. Jager, B. A. Dmitriev and E. T. Rietschel, *Eur. J. Biochem.*, 1991, **198**, 697–704.
- 36 H. Nikaïdo, *Microbiol. Mol. Biol. Rev.*, 2003, **67**, 593–656.
- 37 J. S. Lam, L. L. Graham, J. Lightfoot, T. Dasgupta and T. J. Beveridge, *J. Bacteriol.*, 1992, **174**, 7159–7167.
- 38 H. Y. Yeh and D. M. Jacobs, *J. Bacteriol.*, 1992, **174**, 336–341.
- 39 J. R. Robbins, D. Monack, S. J. McCallum, A. Vegas, E. Pham, M. B. Goldberg and J. A. Theriot, *Mol. Microbiol.*, 2001, **41**, 861–872.
- 40 Y. A. Knirel, E. V. Vinogradov, N. A. Kocharova, N. A. Paramonov, N. K. Kochetkov, B. A. Dmitriev, E. S. Stanislavsky and B. Lanyi, *Acta. Microbiol. Hung.*, 1988, **35**, 3–24.